THE JOURNAL OF PHYSICAL CHEMISTRY C

Article

pubs.acs.org/JPCC

Intraexciton Transitions Observed in High Stability Doped Single-Wall Carbon Nanotube Films and Solutions

Neale O. Haugen, Adam B. Phillips, Tieneke E. Dykstra, Suneth Watthage, Michael J. Heben,* and Randy J. Ellingson*

Wright Center for Photovoltaics Innovation and Commercialization, Department of Physics and Astronomy, The University of Toledo, 2801 West Bancroft Street, Toledo, Ohio 43606, United States

Supporting Information

ABSTRACT: Normally hidden excited state transitions were observed in large diameter single-walled carbon nanotubes for the first time by controlling the degree of doping. With increased doping, the normally observed photoinduced bleach (PB) signal associated with the creation of excitons switched to a photoinduced absorption (PA). A delay in the onset of the PA signal made it clear that the absorption was due to an intraexcitonic transition. The study was afforded by the development of novel methods that allowed samples to be reproducibly and stably prepared in specific states. Our results further the understanding of the photophysics of large diameter single-walled carbon nanotube materials, which are promising for a variety of optoelectronic applications.

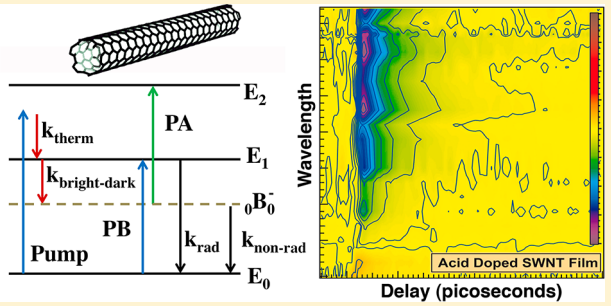

INTRODUCTION

Single-wall carbon nanotubes (SWNTs) have been advanced for use in a variety of electronic and optoelectronic applications owing to many desirable traits including solution processability,[1−3] mechanical flexibility,[4] high carrier mobility,[5] transparency in the infrared spectral region,[6] and large nonlinear susceptibilities.[7] With respect to photovoltaics technology, SWNT films have been used as contacts in thin film,[8−10] organic,[4,11] and crystalline Si photovoltaic (PV) devices.[12,13] SWNTs are also being pursued as active elements in PV devices.[14−16] In particular, semiconducting SWNTs (s-SWNTs) are of great interest due to high absorption coefficients[17] and excitonic transitions[18] that span the visible and near IR portions of the solar spectrum. In photovoltaics, the photoexcitation relaxation mechanisms and dynamics are of paramount importance, with the focus being on the semiconducting SWNT allotropes. As with other PV materials and devices, the potential energy increase created by light absorption is harvested only if the photoexcited carriers can be separated before relaxation processes return the system to the ground state.

Ultrafast transient absorption (TA) spectroscopy is a valuable technique for assessing the photoexcitation relaxation dynamics in SWNT materials and has proven effective for investigating the dynamics of carrier cooling,[19−21] recombination,[22] and free carrier generation[23] in SWNT solutions[21,22,24−27] and films. Due to widespread commercial availability and easily observed optical transitions in the visible and near-infrared portion of the optical spectrum, the vast majority of TA studies to date have been performed on small diameter (0.8−1.2 nm) SWNTs produced by chemical vapor decomposition.[14,26,28−34] In contrast, very little work has been done on larger diameter (1.2−1.6 nm) tubes that are produced by pulsed laser vaporization (PLV). PLV tubes are of great interest for optoelectronic applications due to their lower defect densities. Moreover, their larger diameters may offer advantages in photonic, electronic, and solar energy conversion applications.[2] For example, large diameter tubes have higher carrier mobilities and lower Schottky barriers when interfaced to metal contacts, suggesting better performance in next generation field effect transistors. With respect to solar energy conversion, large diameter tubes provide more complete absorption in the infrared and the possibility of multiple exciton generation in the visible portion of the spectrum,[27] as well as high conductivity in functional contacts.[10] Furthermore, large diameter tubes possess optical transitions that offer complete coverage of all wavelength bands used in fiber-optic telecommunication technologies.

There are several reasons for the lack of ultrafast photophysical data for PLV tubes. First, due to their larger diameters, the first semiconducting excitonic transitions (E1) occur at relatively long wavelengths (1.3−2 μm) that are challenging to access experimentally. Moreover, the optical spectra are congested with contributions from multiple species for PLV tubes because of a larger number of possible tube species at larger diameters.[35] Finally, large diameter tubes are more sensitive to the environment than their smaller diameter

Received: July 29, 2014
Revised: September 18, 2014
Published: October 6, 2014

counterparts (*vide infra*), so the intrinsic photophysics may be obscured by surface effects related to, e.g., doping.

In this report, we compare the steady-state and transient optical absorption spectroscopy of PLV SWNTs in solution and in spray-deposited films. In solution, steady-state absorption spectroscopy shows SWNTs to be well isolated from interaction with the aqueous solvent when solubilized with sodium carboxymethyl cellulose (CMC). In contrast, sodium dodecyl sulfate (SDS) suspended SWNTs show E1 bleaching due to charge polarization doping by the aqueous solvent. Consistently, transient absorption measurements of CMC-suspended SWNTs display a strong photoinduced bleach (PB) signal as expected for population-induced state filling of the E1 transitions, while SDS-suspended SWNTs display an equally strong but unanticipated photoinduced absorption (PA). Ultrasonically sprayed PLV SWNT films prepared from CMC dispersions initially show only a PB signal similar to that seen for CMC solution, but removal of the CMC surfactant by exposure to nitric acid causes the PB signal to be converted to a PA. The PA can then be switched to a PB by heating the film in air to remove the residual acid. After heating, equilibration of the film in laboratory air causes the PB signal to slowly return to a PA signal over the course of hours. The slow conversion is due to reprotonation of surface oxide species by reaction with water vapor in lab air. During this slow conversion, ultrafast TA spectroscopy revealed that the PA signal occurs later in time than does the PB. The PA signal can be assigned to an intraexcitonic transition from a dark state associated with the E1 manifold to an excited E2 state. The dark state is only populated following an E1 transition, which gives rise to the normally observed PB signal. Doping reduces the oscillator strength of the PB signal and allows the PA to dominate. Population of the dark state may be assisted by localized charge centers associated with protonation and/or the presence of the oxygen complexes. Though our focus is on PLV tubes for the reasons discussed above, this study is the first to probe the carrier relaxation dynamics as a function of doping in any type of SWNT film. Interestingly, if the heating and cooling is done in an oxygen-free environment, the surface oxides are completely removed; the surface is kinetically stable against reoxidation; and reprotonation does not occur over the course of several months.

EXPERIMENTAL SECTION

SWNTs were synthesized by a modified version of the method outlined by Dillion et al.[36] and refluxed in nitric acid to remove metals. Solids were collected by filtration to form papers and further purified by combustion of the non-nanotube carbon phases in flowing CO_2 at 900 °C.[36] Purified SWNT papers were dispersed in aqueous solutions of 1% (mg/mL) sodium carboxymethyl cellulose (CMC) or sodium dodecyl sulfate (SDS) using probe sonication with a Fisher Sonic Dismembrator, model 550, with a 1/4" tip, at 100% amplitude for 30 min. The as-synthesized SWNTs exhibited lengths of 1−4 μm prior to sonication. After sonication the tube lengths were reduced to an average of 1 μm, with tube lengths as short as 300 nm measured via atomic force microscopy (AFM). As-received D_2O (Cambridge Isotope Laboratories, pH = 7) was the solvent for solution-based measurements, which were performed in 2 mm cuvettes. Films were prepared by ultrasonic spraying via a Sonotech Impact ultrasonic spray head of SWNTs dispersed with 1% (mg/mL) CMC in deionized H_2O (pH = 7) onto glass microscope slides that were heated to 140 °C during the deposition.[2] Sets of four to five films were sprayed in the same deposition run to provide enough samples for comparative experiments. CMC was removed from the as-sprayed films by soaking overnight in 4 M HNO_3 at room temperature. After surfactant removal, films were rinsed with deionized water and dried at 80 °C. Collapsed film thicknesses were ∼160 nm for the thick sets of film and ∼42 nm for the thin sets of films, as determined by optical profilometry. Strongly absorbed nitric acid was removed by heating samples on a hot plate with a surface temperature of 250 °C for 30 min in either ambient air or a dry nitrogen glovebox. Films were stored in ambient air. Steady-state absorption measurements were performed using a PerkinElmer Lambda model 1050 spectrometer. Transient absorption measurements were performed using a system based on an amplified Ti:sapphire Solstice (Spectra Physics) laser pumping two TOPAS optical parametric amplifiers. Pump and probe pulse widths were ∼150 fs. The excitation density of the pump laser was between 5×10^{13} and 2×10^{14} photons pulse^{-1} cm^{-2} for all TA experiments corresponding to between 20 and 80 excitons/(μm of tube length) (Figure S1, Supporting Information). The pump wavelength of 1215 nm (1.02 eV) was chosen to lay between the E1 and E2 excitonic transition peaks (see Figure 1). The

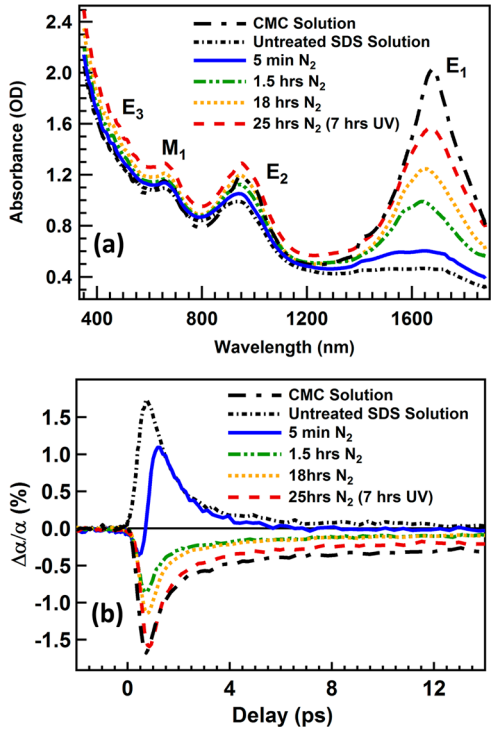

Figure 1. PLV SWNTs suspended in CMC and SDS dispersions examined by (a) steady-state and (b) transient optical absorption spectroscopies (λ pump = 1215 nm, λ probe = 1690 nm). Times are cumulative bubbling time, and after each period the sample was allowed to re-equilibrate.

TA data are presented as $\Delta\alpha/\alpha$, so the response is normalized to the linear absorption coefficient at the probe wavelength prior to arrival of the pump beam. The repetition rate of measurement was 2 kHz.

RESULTS AND DISCUSSION

Surfactant-Suspended SWNT Solutions. Steady-state and transient absorption optical spectra for solutions containing

dx.doi.org/10.1021/jp507653j | J. Phys. Chem. C 2014, 118, 25253−25260

PLV SWNTs are shown in Figures 1a and 1b, respectively. When suspended with the organic polymer CMC, PLV tubes are well dispersed and isolated from one another and do not flocculate on the time scale of months. The steady-state absorption spectrum (Figure 1a) shows prominent contributions from the E1 and E2 excitonic transitions for the s-SWNTs in the sample, as well as features associated with the first (M1) transition for the m-SWNTs and higher energy E3 transitions for the s-SWNTs. As discussed previously, the E1 band is more spectrally congested in PLV SWNTs, and individual (n,m) species in the sample are difficult to discern (see Figure S2, Supporting Information). Note that this is not evidence for tube−tube contact or bundling. First, note that the bandwidth of the van Hove singularity involved in each ground-state-to-E1 transition is ∼25 meV.[37] Since the number of possible species in the PLV diameter range is larger (∼36) than in the HiPCO diameter range (∼26) and the average energy difference between the E1 transitions of PLV tubes of neighboring diameter is ∼30 versus ∼60 meV for HiPCO tubes, the optical transitions for the distribution of PLV tubes are strongly overlapping. The lack of tube−tube contact in CMC-suspended PLV SWNTs is supported by the measured lifetimes for the TA transients (*vide infra*).

In addition to being isolated from one another, CMC-suspended tubes show no sign of interaction with the aqueous solvent environment. In contrast, the entire E1 absorption envelope is almost completely absent in the absorption spectrum for the SDS-suspended SWNTs (Figure 1a). The loss of oscillator strength for the E1 transitions is due to doping associated with protonation by the solvent of oxygen species chemisorbed on the nanotube walls.[38,39] In doping, electron density is withdrawn from the delocalized HOMO and localized at the protonation site. The net effect is a p-type doping that can be described as a Fermi level shift toward the valence band.[40] Spectroscopically, the oscillator strength for the HOMO−LUMO E1 transition is dramatically reduced. The degree of quenching observed is surprising considering that the samples were in neutral D_2O, but the results are consistent with previous NMR studies on the interactions of PLV SWNTs with water.[41] Comparable E1 quenching across the range of smaller diameter HiPCO SWNTs in SDS dispersions requires a much lower pH of 2.5.[38] Though the doping mechanism is apparently the same for both small and large diameter tubes, the protonated complexes are much more readily formed on larger diameter SWNTs due to a combination of a higher stability for the surface bound oxygen species[38,39] and a more labile surfactant sheath that readily admits solvent species.[42] It is surprising that doping is not observed for the CMC-suspended SWNTs because the CMC and SDS samples were prepared similarly, and oxygen groups are likely present in both cases. The strong binding of the cellulosic polymer to the SWNT surface evidently excludes water and inhibits formation of the protonated complex.

Because the SDS surfactant sheath is labile,[42] hydronium ions can readily access the SWNT surface and protonate surface-bound oxygen species. With an effective excess of hydronium ions, the degree of doping has been shown to be strongly dependent on the concentration of surface oxygen species.[38] Figure 1a shows the evolution of the absorption spectra as N_2 gas is bubbled through the SDS-suspended sample and oxygen is desorbed from tube walls. After 1.5 h of N_2 bubbling, the E1 transitions reappear with a peak wavelength that is slightly blue-shifted relative to the CMC data. This is consistent with larger diameter tubes in the distribution having a higher affinity for chemisorbed oxygen.[38,39] After 25 h of N_2 bubbling (including 7 h under ultraviolet light exposure to photostimulate desorption), the E1 transition envelope is re-established, and the peak position returns to the unshifted position. After a long period of bubbling the doping state of the tubes should reach equilibrium with the surrounding environment wherein weakly adsorbed oxygen is desorbed and purged, while more strongly held species remain adsorbed to the SWNT sidewall. Presumably, the E1 absorbance intensity does not reach the full intensity seen in the CMC sample due to a small number of remaining tightly bound species that could be removed with more aggressive efforts (i.e., heating or more intense UV photodesorption). We believe that the E1 absorbance fails to fully recover due to slow oxygen desorption from the PLV tubes, which is consistent with studies on HiPCO tubes in which stronger oxygen chemisorption was seen for the larger diameter tubes in the distribution.[38]

Figure 1b shows the companion transient absorption data. The pump wavelength was chosen to excite tubes between the E2 and E1 absorption features to avoid resonant excitation and instead broadly couple into the high-energy tail of the E1 envelope (λ_{pump} = 1215 nm). The probe wavelength was adjusted to the peak of the E1 absorption feature, which is close to the E1 absorption of several tubes in the PLV SWNT sample (Figure 2).[35] For the CMC-suspended tubes, a transient

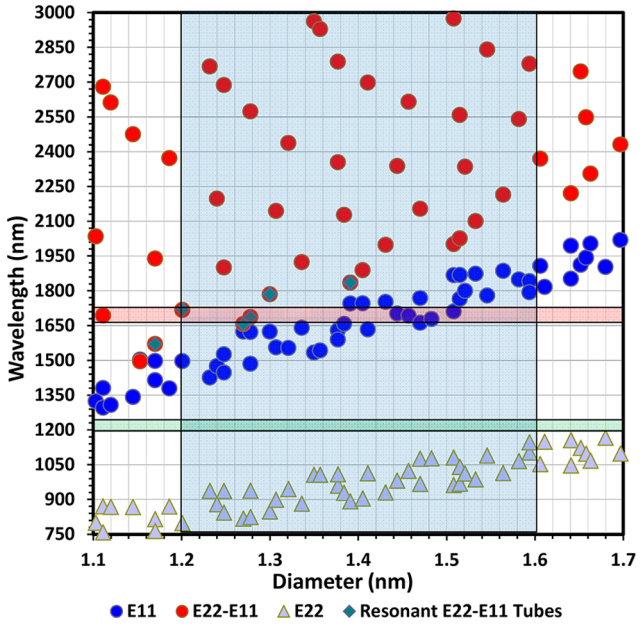

Figure 2. Transition energies for the E1, and E1 to E2 transitions for SWNTs in the PLV diameter range (1.2−1.6 nm) following the assignments by Bachilo and Weisman.[35] Vertical black lines at 1.2 and 1.6 nm indicate the approximate limits of the tube diameters within our samples. Green diamonds indicate E1 → E2 transitions resonant within the range of our probe measurements (see Figure 5b).

photoinduced bleach (PB) is detected as the transmission of the sample is increased by state filling of the E1 exciton, as has been observed by others.[20,37,43] A biexponential fit to the decay of the signal indicates two lifetimes with fast (0.8 ± 0.2 ps, ∼90%) and slow (1.1 ± 0.2 ns, ∼10%) components (see Supporting Information). Due to the lack of tube−tube interactions which could lead to fast energy transfer and the low excitation fluences which make fast exciton−exciton

dx.doi.org/10.1021/jp507653j | J. Phys. Chem. C 2014, 118, 25253−25260

recombination unlikely, we can assign the fast decay to rapid nonradiative interband recombination within states comprising the E1 manifold.[31,44] The origin of the slow decay component[26,45,46] is less clear but could be associated with the intrinsic radiative lifetime of defect-free PLV SWNTs,[47,48] may reflect coupling of singlet and triplet states,[49,50] or be due to slow depopulation of the "dark" dipole-forbidden state that sits at lower energy with respect to the "bright" dipole-allowed transition.[26]

The TA data for the PLV SWNTs dispersed with SDS are distinctly different. In this case, a prompt PA signal, rather than a PB, is observed. The origin of the PA is most likely due to intraexciton E1 to E2 transitions for specific SWNTs in the PLV distribution. Intersubband optical transitions are strictly forbidden for the single particle (electron or hole) case.[43] Such transitions have been observed with smaller diameter HiPCO tubes but have not yet been reported for PLV SWNTs. Korovyanko et al.[43] excited HiPCO SWNT films above the E2 transition and measured the TA behavior over a wide spectral range with a broad-band probe. A PB signal was observed over the range of the E1 transitions as expected for state filling, but a PA was observed at longer wavelengths. Relaxation of the photoexcitation to the lowest E1 state offered the possibility of a photoexcited transition from the E1 manifold to a state within the E2 manifold and a corresponding PA at a lower energy (see Figure 2). Since the energy differences, E2 minus E1, are more varied across a diameter range than are the E1 values themselves, Yang et al.[37] used the lifetime of the transient at the E2−E1 energy to characterize the lifetime of the E1 exciton. This approach allowed single tube-type data to be straightforwardly extracted from measurements on polydisperse HiPCO samples.

In our case, doping reduces the oscillator strength for the E1 excitations and allows a PA signal associated with the E1 → E2 transition for certain smaller diameter tubes to be observed. Figure 2 shows the energies for the E1, and E2 minus E1, transitions for SWNTs in the PLV diameter range (1.2−1.6 nm) following the assignments by Bachilo and Weisman.[35] The two horizontal bars correspond to the pump (1215 nm, 40 nm full width at half-maximum (fwhm), green) and probe (1690 nm, 60 nm fwhm, red) wavelengths used in this study. At the selected probe wavelength, approximately 1/2 of the tubes in the PLV distribution have E1 transitions that are too high in energy to be measured. Considering the bandwidth of the probe wavelength, ∼6 tubes have E1 transitions that are nearly resonant. Because the doping is strongly diameter dependent, the E1 transitions in these resonant tubes, which are on the large side of the diameter distribution, are expected to be more strongly quenched than in the smaller diameter tubes in the distribution. If we consider that the E1 transition is incompletely quenched in these smaller diameter SWNTs, the observed PA can be assigned to intraexciton E1 → E2 transitions in these specific tubes. The (15,2) and (16,0) tubes with diameters of 1.270 and 1.278 nm, respectively, have E1 *and* E1 → E2 transition energies that are near the 1690 nm probe wavelength and could account for the PA seen at wavelengths as short as 1570 nm.

With N_2 bubbling and the application of ultraviolet light to accelerate oxygen desorption from the SDS-suspended SWNTs, the PA signal is slowly converted back to a dominant PB signal. After approximately 18 h the recovery of the E1 absorption feature reached equilibrium with the N_2-rich and O_2-deficient environment. The slight blue shift of the E1 absorption peak is likely a result of a small population of strongly adsorbed dopant species, possibly at defect sites or tube ends, remaining on the tubes following the removal of all of the weakly adsorbed dopant species. In an attempt to fully remove all the dopant species from the SWNT surfaces, 7 h of UV photoexcitation was employed. This succeeded in decreasing the doping (increasing the E1 transition strength), to a nearly intrinsic state.

The lifetime of the transient photoresponse also changes with doping (see Figure 1b). While the CMC solution shows an E1 PB with a nonzero signal at 14 ps delay, the SDS solution shows a clear PA signal and no measurable longer-lived component beyond ∼10 ps. Upon bubbling of N_2, the PA begins immediately to convert to a PB with a long-lived (∼1 to 2 ns) component (see Figure S4, Supporting Information). The fast component of the decays (PA and PB) remains nearly the same in all cases from the fully oxygenated SDS to the CMC solution. The lack of a slow component in the doped sample may be indicative of thermalization followed by fast quenching of the excitons through interactions with dopant complexes on the surface. This interpretation is further reinforced by noting that upon full deoxygenation of the SDS solution the PB begins to exhibit a low amplitude slow component. The molecular picture is that the SDS surfactant allows water to access the surface of the SWNTs where it is able to protonate the adsorbed molecular oxygen. The removal of the oxygen from the solution then dedopes the surface of the SWNTs. This conversion from doped to undoped as a function of oxygenation is not seen in the CMC solution sample since the CMC is known to exclude either oxygen or water from the surface. Most likely water is excluded since the SWNT samples were prepared in air and are assumed to already have oxygen adsorbed on the SWNT sidewalls.

We note that Ostojic et al.[31] did not report photoinduced absorption in TA studies of the effect of doping on HiPCO SWNTs. As stated previously, the doping is weaker in HiPCO SWNT populations due to the smaller diameters and larger band gap energies as compared to PLV SWNTs. They reported a loss of the slow decay component which may be attributed to an onset of doping such as we have observed, but the doping was evidently insufficient to induce full extinction of the E1 absorption band.

SWNT Films. SWNT films were investigated to further understand the effects of doping and the origin of the PA signal. Figures 3a and 3b compare the steady-state and transient absorption data, respectively, for several SWNT films and SWNTs suspended by CMC in solution. In Figure 3a, the spectra for the films were plotted as measured, while the CMC solution data were normalized to the rising high-energy E3 region and π plasmon edge of the data set. This was done to account for the concentration difference between the films and the CMC solution. The spectrum for the as-sprayed film closely matches the CMC reference solution spectrum across the M1 and E2 envelopes, but the E1 envelope is broadened, red-shifted, and reduced in amplitude. Evidently, even the relatively low temperatures employed during the spray deposition and film drying processes (140 and 80 °C, respectively) allowed some tube−tube coupling and perhaps a small amount of surface oxygen protonation and concomitant doping. However, there is insufficient thermal energy to allow large-scale SWNT rearrangement and any significant degree of bundling.[2] The as-sprayed film displays a PB signal (Figure 3b) that is quite similar to the CMC solution data as expected for state filling.

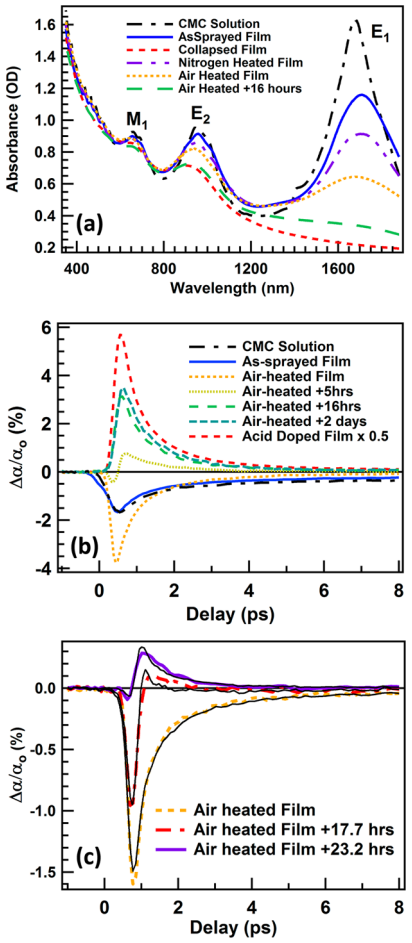

Figure 3. Optical absorption: (a) steady-state spectra of SWNT films and solution in different doping states and (b) time-resolved transient absorption changes as measured at the E1 exciton peak (1690 nm) following excitation at 1215 nm. (c) Fitting of the mixed signal from the partially doped films; fits are a linear combination of the fully doped and N_2-heated transient responses. Fitting results are reported in Table 1.

When the data are normalized for the differences in intensity, it can be seen that the full amplitude of the long-lived transient for samples in CMC solution is retained for the film.

The CMC surfactant was removed from the as-sprayed film by soaking overnight in 4 M HNO_3.[2] The process causes the film to collapse as the CMC is digested and dissolved, and the thickness of the film is reduced to ∼7% of its initial value. Simultaneously, the high acid concentration produces strong p-type doping due to protonation of chemisorbed oxygen species.[32,39,40] Thus, a percolating network of doped SWNTs is formed, and the sheet resistance of the film decreases by 3−4 orders of magnitude.[2] As with the SDS-suspended SWNTs in solution, the introduction of free holes into the valence band of the doped s-SWNTs bleaches the E1 band. In this case, however, the E1 absorption feature is removed completely, and the E2 transition is more strongly affected (Figure 3a). The companion TA data (Figure 3b) show an intense PA signal that can be expected from the results for the SDS-suspended SWNTs (Figure 1b) and the much higher degree of doping here. The near-complete bleaching of the E1 band and the partial bleaching of the low energy side of the E2 band in the steady-state absorption data suggest that no E1 excitons would be available to participate in the E1 → E2 transition if we consider resonant excitation only. However, even the small degree of absorption that remains at 1215 nm is able to prepare a sufficient population of E1 excitons, through nonresonant excitation, that may then be further excited by the 1690 nm probe to generate a PA signal.

The E1 bleach in acid-doped SWNT films persists for more than 4 months in laboratory air, indicating the presence of strongly bound acid species and a stable equilibrium for the protonated complexes. In similarity to changes in doping due to purging the SDS solutions with N_2, the E1 absorption feature of the films can be restored by decomposing the complexes that are responsible for the doping. In this case, heating a strongly doped film in air to 200 °C for 30 min temporarily and partially restores the original E1 absorption band (Figure 3a). Here, rather than reducing the surface concentration of chemisorbed oxygen species by bubbling N_2, the films are dedoped by thermal deprotonation of the complexes, while the oxygen species are still present. This latter point may be concluded from experiments designed to separate the oxygen and protonation kinetics (see Supporting Information). After thermal decomposition of the doping complex, the E1 feature is slowly rebleached as the surface oxygen species are reprotonated by water in lab air. The time constant for this process depended on the film thickness and the humidity. While a significant change in the ratio of the PA and PB components occurs over the course of hours, time-dependent TA measurements can be acquired in 20 min (Figure 3b and 3c), and thus the transition can be tracked. Note that the TA response for SDS-suspended SWNTs was fully converted from a PA to a PB with as little as 1.5 h of N_2 bubbling (Figure 1b) in solution.

Examination of films that are slowly changing allows for direct comparison of the relative dynamics of the PA and PB processes. Additionally, the reduced sample thickness for the films (∼100 nm) vs the solutions (1 mm cuvette path length) improves the measurement's temporal resolution. Within an extended solution sample, the probe beam which is noncollinear with the pump beam instantaneously samples a range of delays depending on the angle of noncollinearity. As a result, the film-based measurements result in an improvement in the time resolution by ∼200 fs and allow for more accurate measurement of the dynamics. Our observed influence on time resolution is somewhat larger, perhaps owing to group velocity dispersion between pump and probe wavelengths within the solution sample. For example, we note that the fwhm of the PA decay for SWNT films is ∼0.75 ps (Figure 3b), while the similar transient is ∼1.5 ps wide for SDS-suspended SWNTs (Figure 1b). Thus, the use of films allows us to more clearly observe that the PA follows the PB process (Figure 3c). In fact, the overall response for a wide range of doping states can be modeled quite well using the linear combination of three exponentials comprising: (i) a single ∼140 fs fast rise time for both the PA and PB processes, (ii) fast (0.61 ps) and slow (2.2 ps) components for the decay of the PB process, and (iii) fast (0.63 ps) and slow (3.3 ps) components for the decay of the PA process. The pure PB dynamics were measured from films that were heated in N_2 to desorb all oxygen species and therefore were not reprotonated in lab air over the course of many months (see Supporting Information), while the pure PA components were extracted from measurements of acid-doped films (see Table 1).

Evidently, the states involved with the PB response must first be populated before the PA can be observed. The relative

dx.doi.org/10.1021/jp507653j | J. Phys. Chem. C 2014, 118, 25253−25260

Table 1. Results of Biexponential Fits to the TA Decays of the Doped and Heated Samples[a]

	time constant (ps)		$\Delta\alpha/\alpha$ (%)			
sample description	fast	slow	fast	slow	PA (%)	PB (%)
pure PB (heated in N_2)	0.61	2.2	−3.7	−1.0	0	100
pure PA (acid-doped)	0.63	3.3	6.0	2.0	100	0
air Heated	NA		NA		17	44
air Heated +17.7 h	NA		NA		23	39
air Heated +23.2 h	NA		NA		30	36

[a]The mixed signals were fit to a linear combination of the full-scale signals. Exposure times to laboratory air are indicated for the last two air-heated samples.

dynamics suggest that this is true even when the PB cannot be observed. This is the case for the acid-doped films, where the PA signal dominates the TA response, but only after a short delay. To investigate the possibility of free carrier absorption accounting for the observed PA the mid-infrared photoresponse of our doped SWNT films was also measured. No detectible PA was observed in the range of 3−5 μm. Therefore, we conclude that free carrier absorption cannot explain the behavior we observe in our doped and partially doped SWNT samples. To explain this behavior, we consider that the E1 → E2 transition may first require a bright-to-dark exciton transition. In this model, photoexcitation at 1215 nm creates excitons within the high-energy tail of the E1 exciton absorption band which rapidly cools toward the E1 absorption edge and equilibrates within the E1 manifold of states. Ma et al. have described the theoretical electronic structure of states near the E1 absorption edge, which includes both optically allowed and dark states, labeled as $_0A^-_0$, and $_0B^-_0$.[51] Their experimental studies with HiPCO SWNTs indicated a dark-to-bright state transition time of ∼160 fs, consistent with the time scale on which we observe the switch from PB to PA in partially doped SWNT samples. Utilizing the electronic structure described by Ma et al., we propose the scheme shown in Figure 4 to explain the processes responsible for the dynamical features we observe. It is interesting to consider that the presence of oxygen species and the degree of protonation may affect the equilibration dynamics for the states comprising the E1 manifold. However, the experiments described here cannot directly comment on this matter.

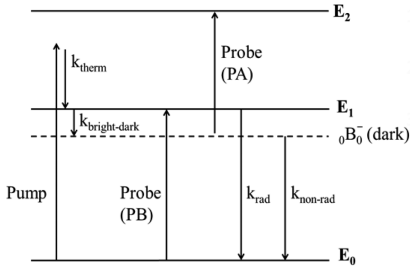

Figure 4. Model of exciton behavior based on TA measurements: E0, E1, and E2 represent the ground state and first and second exciton levels. Pump photons create hot E1 excitons, which cool at a rate k_{therm} and recombine at rates characterized by k_{rad} and k_{nonrad}. Thermalized E1 bright excitons generate a PB when the E1 band is probed. Bright E1 excitons transition to the dark state ($_0B^-_0$) at rate $k_{bright\text{-}dark}$. Excitons within the dark exciton state may more strongly absorb probe photons, promoting them to the E2 state.

To examine the E1 → E2 transitions over a broader range of tubes species, we investigated stable acid-doped and N_2 heated films by TA with the probe wavelength varied from 1500 to 1820 nm. Figure 5a shows the data for the N_2 heated film

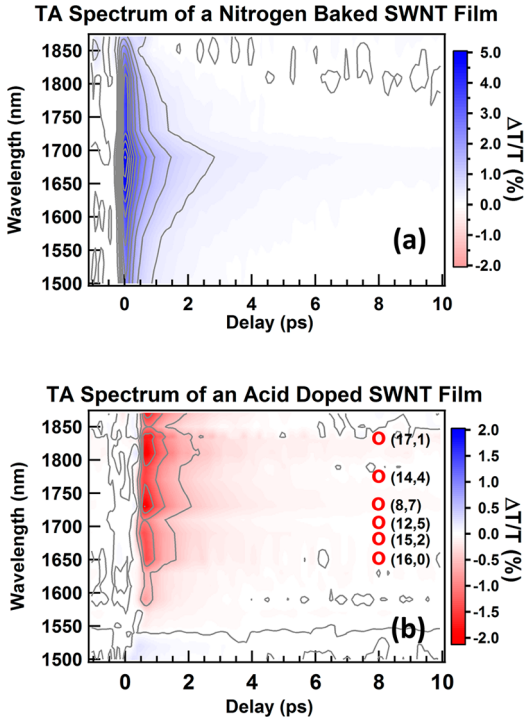

Figure 5. Transient spectral response of the thick sprayed films, after (a) heating in nitrogen and (b) soaking in 4 M nitric acid for 18 h. Note the crossover from the PA to the PB at 1540 nm in the acid-doped film. Tubes with resonant E1 → E2 intraexciton transitions within the probe range are identified by red circles in (b).

where a pure PB response is observed for every probe wavelength. Here, the intensity of the PB signal follows the linear absorption response with a peak at ∼1690 nm. In contrast, Figure 5b shows the data for the strongly doped samples where PA signals are dominant. The red circles in the plot mark the approximate wavelengths of E1 → E2 transitions for tube species with E1 transitions falling within the E1 band for our PLV distribution.[35] The good correspondence between the expected and measured locations of the intraexcitonic transitions indicates that our analysis accurately describes the photophysics in these PLV SWNTs. We note that the appearance of a small PB signal at ∼1520 nm is consistent with E1 excitation of the (11, 7) tubes species that is at the small diameter edge of the PLV diameter range. In this case, there is no corresponding intraexciton transition that can be excited (see Figure 2).

PLV SWNT films and solutions have been employed using linear absorption and ultrafast transient absorption spectroscopy to reveal how static and dynamic optical properties vary with the degree of doping by protonation. Our transient absorption studies revealed that while dedoped SWNT films show the expected bleach of the E1 transitions due to state filling by the E1 exciton population doped SWNT films show a clear photoinduced absorption signal. Both the PB and the PA signal decay with nearly identical dynamics. The PA signal arises from an intraexciton transition from the dark state within the E1 absorption edge. Since the ensemble of intraexciton transitions

dx.doi.org/10.1021/jp507653j | J. Phys. Chem. C 2014, 118, 25253−25260

for PLV-SWNTs overlaps substantially with the E1 exciton absorption band, the PA contribution to the TA signal is present even in undoped samples but is dominated by the PB signal associated with E1 population state filling. We are able to probe the ultrafast transient absorption signal at the peak of the E1 band, which simultaneously allows probing of the PA signal for doped samples. Analysis of the mixed-polarity (PB and PA) signal in partially doped samples reveals evidence for the delayed onset of intraexciton absorption relative to cooling to the bright E1 state. It was also found that doped films can be thermally dedoped by heating to temperatures >180 °C. Doped SWNT films thermally dedoped in air do not remain stably dedoped, whereas films dedoped in a dry N_2 environment are stably dedoped, with no propensity to redope in laboratory air (within a time frame of 10 months). Such a resistance to doping demonstrates an important effect for electronic functional layers such as absorber or transparent conductor layers in solar cells and will be more completely discussed in a subsequent publication.

■ ASSOCIATED CONTENT

Ⓢ Supporting Information

Studies investigating the power dependence of the transient absorption signal in PLV SWNT collapsed films, UV−vis−NIR absorption spectra showing the unresolved nature of the individual E_1 absorption features of the various SWNT species present in the PLV samples, a study of the dependence of the wavelength of the E_1 peak on the doping state of the SWNT ensemble in solution, transient absorption data showing the long-lived component present in isolated undoped PLV SWNTs and its disappearance following collapse of the SWNT films, time-dependent studies of the change in the transient photoresponse with time in air (i.e., redoping times for various treatments), and finally a graph of the same data as Figure 3c but with the full-scale PA and PB signals shown. This material is available free of charge via the Internet at http://pubs.acs.org.

■ AUTHOR INFORMATION

Corresponding Authors

*E-mail: randy.ellingson@utoledo.edu. Phone: 419-530-3874

*E-mail: michael.heben@utoledo.edu. Phone: 419-530-3870.

Notes

The authors declare no competing financial interest.

■ ACKNOWLEDGMENTS

The authors gratefully acknowledge the support of the Air Force Research Laboratory under contracts F9453-08-C-0172 and F9453-11-C-0253, support from the NREL Nano Bio Program under Contract #DE-AC36-08GO28308, and start-up funds provided through the University of Toledo's Wright Center for Photovoltaic Innovation and Commercialization (www.pvic.org).

■ REFERENCES

(1) Wu, Z.; Chen, Z.; Du, X.; Logan, J. M.; Sippel, J.; Nikolou, M.; Kamaras, K.; Reynolds, J. R.; Tanner, D. B.; Hebard, A. F. Transparent, Conductive Carbon Nanotube Films. *Science* **2004**, *305*, 1273−1276.

(2) Tenent, R. C.; Barnes, T. M.; Bergeson, J. D.; Ferguson, A. J.; To, B.; Gedvilas, L. M.; Heben, M. J.; Blackburn, J. L. Ultrasmooth, Large-Area, High-Uniformity, Conductive Transparent Single-Walled-Carbon-Nanotube Films for Photovoltaics Produced by Ultrasonic Spraying. *Adv. Mater.* **2009**, *21*, 3210−3216.

(3) Ramuz, M. P.; Vosgueritchian, M.; Wei, P.; Wang, C.; Gao, Y.; Wu, Y.; Chen, Y.; Bao, Z. Evaluation of Solution-Processable Carbon-Based Electrodes for All-Carbon Solar Cells. *ACS Nano* **2012**, *6*, 10384−10395.

(4) Rowell, M. W.; Topinka, M. A.; McGehee, M. D.; Prall, H. J.; Dennler, G.; Sariciftci, N. S.; Hu, L. B.; Gruner, G., Organic Solar Cells with Carbon Nanotube Network Electrodes. *Appl. Phys. Lett.* **2006**, *88*.

(5) Dürkop, T.; Getty, S. A.; Cobas, E.; Fuhrer, M. S. Extraordinary Mobility in Semiconducting Carbon Nanotubes. *Nano Lett.* **2003**, *4*, 35−39.

(6) Borondics, F.; Kamarás, K.; Nikolou, M.; Tanner, D. B.; Chen, Z. H.; Rinzler, A. G. Charge Dynamics in Transparent Single-Walled Carbon Nanotube Films from Optical Transmission Measurements. *Phys. Rev. B* **2006**, *74*, 045431.

(7) Maeda, A.; Matsumoto, S.; Kishida, H.; Takenobu, T.; Iwasa, Y.; Shiraishi, M.; Ata, M.; Okamoto, H. Large Optical Nonlinearity of Semiconducting Single-Walled Carbon Nanotubes under Resonant Excitations. *Phys. Rev. Lett.* **2005**, *94*, 047404.

(8) Contreras, M.; Barnes, T.; van de Lagemaat, J.; Rumbles, G.; Coutts, T. J.; Weeks, C.; Glatkowski, P.; Levitsky, I.; Peltola, J. In Application of Single-Wall Carbon Nanotubes as Transparent Electrodes in Cu(in,Ga)Se2-Based Solar Cells, Photovoltaic Energy Conversion, *Conference Record of the 2006 IEEE 4th World Conference on*, May 2006; 2006; pp 428−431.

(9) Barnes, T. M.; Wu, X.; Zhou, J.; Duda, A.; van de Lagemaat, J.; Coutts, T. J.; Weeks, C. L.; Britz, D. A.; Glatkowski, P. Single-Wall Carbon Nanotube Networks as a Transparent Back Contact in Cdte Solar Cells. *Appl. Phys. Lett.* **2007**, *90*, 243503.

(10) Phillips, A. B.; Khanal, R. R.; Song, Z.; Zartman, R. M.; DeWitt, J. L.; Stone, J. M.; Roland, P. J.; Plotnikov, V. V.; Carter, C. W.; Stayancho, J. M.; et al. Wiring-up Carbon Single Wall Nanotubes to Polycrystalline Inorganic Semiconductor Thin Films: Low-Barrier, Copper-Free Back Contact to Cdte Solar Cells. *Nano Lett.* **2013**, *13*, 5224−5232.

(11) Pasquier, A. D.; Unalan, H. E.; Kanwal, A.; Miller, S.; Chhowalla, M. Conducting and Transparent Single-Wall Carbon Nanotube Electrodes for Polymer-Fullerene Solar Cells. *Appl. Phys. Lett.* **2005**, *87*, 203511.

(12) Jia, Y.; et al. Nanotube−Silicon Heterojunction Solar Cells. *Adv. Mater.* **2008**, *20*, 4594−4598.

(13) Jia, Y.; Cao, A.; Bai, X.; Li, Z.; Zhang, L.; Guo, N.; Wei, J.; Wang, K.; Zhu, H.; Wu, D.; Ajayan, P. M. Achieving High Efficiency Silicon-Carbon Nanotube Heterojunction Solar Cells by Acid Doping. *Nano Lett.* **2011**, *11*, 1901−1905.

(14) Jain, R. M.; Howden, R.; Tvrdy, K.; Shimizu, S.; Hilmer, A. J.; McNicholas, T. P.; Gleason, K. K.; Strano, M. S. Polymer-Free near-Infrared Photovoltaics with Single Chirality (6,5) Semiconducting Carbon Nanotube Active Layers. *Adv. Mater.* **2012**, *24*, 4436−4439.

(15) Shea, M. J.; Arnold, M. S. 1% Solar Cells Derived from Ultrathin Carbon Nanotube Photoabsorbing Films. *Appl. Phys. Lett.* **2013**, *102*, 243101.

(16) Arnold, M. S.; Zimmerman, J. D.; Renshaw, C. K.; Xu, X.; Lunt, R. R.; Austin, C. M.; Forrest, S. R. Broad Spectral Response Using Carbon Nanotube/Organic Semiconductor/C60 Photodetectors. *Nano Lett.* **2009**, *9*, 3354−3358.

(17) Zhao, B.; Itkis, M. E.; Niyogi, S.; Hu, H.; Zhang, J.; Haddon, R. C. Study of the Extinction Coefficients of Single-Walled Carbon Nanotubes and Related Carbon Materials. *J. Phys. Chem. B* **2004**, *108*, 8136−8141.

(18) Wang, F.; Dukovic, G.; Brus, L. E.; Heinz, T. F. The Optical Resonances in Carbon Nanotubes Arise from Excitons. *Science* **2005**, *308*, 838−841.

(19) Hertel, T.; Moos, G. Electron-Phonon Interaction in Single-Wall Carbon Nanotubes: A Time-Domain Study. *Phys. Rev. Lett.* **2000**, *84*, 5002−5005.

(20) Ichida, M.; Hamanaka, Y.; Kataura, H.; Achiba, Y.; Nakamura, A. Ultrafast Relaxation Dynamics of Photoexcited Carriers in Metallic and Semiconducting Single-Walled Carbon Nanotubes. *J. Phys. Soc. Jpn.* **2004**, *73*, 5.

(21) Dyatlova, O. A.; Köhler, C.; Malic, E.; Gomis-Bresco, J.; Maultzsch, J.; Tsagan-Mandzhiev, A.; Watermann, T.; Knorr, A.; Woggon, U. Ultrafast Relaxation Dynamics Via Acoustic Phonons in Carbon Nanotubes. *Nano Lett.* **2012**, *12*, 2249−2253.
(22) Wang, F.; Dukovic, G.; Knoesel, E.; Brus, L. E.; Heinz, T. F. Observation of Rapid Auger Recombination in Optically Excited Semiconducting Carbon Nanotubes. *Phys. Rev. B* **2004**, *70*, 241403.
(23) Beard, M. C.; Blackburn, J. L.; Heben, M. J. Photogenerated Free Carrier Dynamics in Metal and Semiconductor Single-Walled Carbon Nanotube Films. *Nano Lett.* **2008**, *8*, 4238−4242.
(24) Ostojic, G. N.; Zaric, S.; Kono, J.; Moore, V. C.; Hauge, R. H.; Smalley, R. E. Stability of High-Density One-Dimensional Excitons in Carbon Nanotubes under High Laser Excitation. *Phys. Rev. Lett.* **2005**, *94*, 097401.
(25) Hertel, T.; Zhu, Z.; Crochet, J.; McPheeters, C.; Ulbricht, H.; Resasco, D. Exciton Dynamics Probed in Carbon Nanotube Suspensions with Narrow Diameter Distribution. *Phys. Status Solidi (b)* **2006**, *243*, 3186−3191.
(26) Zhu, Z.; Crochet, J.; Arnold, M. S.; Hersam, M. C.; Ulbricht, H.; Resasco, D.; Hertel, T. Pump-Probe Spectroscopy of Exciton Dynamics in (6,5) Carbon Nanotubes. *J. Phys. Chem. C* **2007**, *111*, 3831−3835.
(27) Wang, S.; Khafizov, M.; Tu, X.; Zheng, M.; Krauss, T. D. Multiple Exciton Generation in Single-Walled Carbon Nanotubes. *Nano Lett.* **2010**, *10*, 2381−2386.
(28) Chen, R. J.; Franklin, N. R.; Kong, J.; Cao, J.; Tombler, T. W.; Zhang, Y.; Dai, H. Molecular Photodesorption from Single-Walled Carbon Nanotubes. *Appl. Phys. Lett.* **2001**, *79*, 2258−2260.
(29) O'Connell, M. J.; Bachilo, S. M.; Huffman, C. B.; Moore, V. C.; Strano, M. S.; Haroz, E. H.; Rialon, K. L.; Boul, P. J.; Noon, W. H.; Kittrell, C.; et al. Band Gap Fluorescence from Individual Single-Walled Carbon Nanotubes. *Science* **2002**, *297*, 593−596.
(30) Bachilo, S. M.; Balzano, L.; Herrera, J. E.; Pompeo, F.; Resasco, D. E.; Weisman, R. B. Narrow (N,M)-Distribution of Single-Walled Carbon Nanotubes Grown Using a Solid Supported Catalyst. *J. Am. Chem. Soc.* **2003**, *125*, 11186−11187.
(31) Ostojic, G. N.; Zaric, S.; Kono, J.; Strano, M. S.; Moore, V. C.; Hauge, R. H.; Smalley, R. E. Interband Recombination Dynamics in Resonantly Excited Single-Walled Carbon Nanotubes. *Phys. Rev. Lett.* **2004**, *92*, 117402.
(32) Cognet, L.; Tsyboulski, D. A.; Rocha, J.-D. R.; Doyle, C. D.; Tour, J. M.; Weisman, R. B. Stepwise Quenching of Exciton Fluorescence in Carbon Nanotubes by Single-Molecule Reactions. *Science* **2007**, *316*, 1465−1468.
(33) Berciaud, S.; Cognet, L.; Lounis, B. Luminescence Decay and the Absorption Cross Section of Individual Single-Walled Carbon Nanotubes. *Phys. Rev. Lett.* **2008**, *101*, 077402.
(34) Blackburn, J. L.; McDonald, T. J.; Metzger, W. K.; Engtrakul, C.; Rumbles, G.; Heben, M. J. Protonation Effects on the Branching Ratio in Photoexcited Single-Walled Carbon Nanotube Dispersions. *Nano Lett.* **2008**, *8*, 1047−1054.
(35) Weisman, R. B.; Bachilo, S. M. Dependence of Optical Transition Energies on Structure for Single-Walled Carbon Nanotubes in Aqueous Suspension: An Empirical Kataura Plot. *Nano Lett.* **2003**, *3*, 1235−1238.
(36) Dillon, A. C.; Gennett, T.; Jones, K. M.; Alleman, J. L.; Parilla, P. A.; Heben, M. J. A Simple and Complete Purification of Single-Walled Carbon Nanotube Materials. *Adv. Mater.* **1999**, *11*, 1354−1358.
(37) Yang, J. P.; Kappes, M. M.; Hippler, H.; Unterreiner, A. N. Femtosecond Transient Absorption Spectroscopy of Single-Walled Carbon Nanotubes in Aqueous Surfactant Suspensions: Determination of the Lifetime of the Lowest Excited State. *Phys. Chem. Chem. Phys.* **2005**, *7*, 512−517.
(38) Strano, M. S.; Huffman, C. B.; Moore, V. C.; O'Connell, M. J.; Haroz, E. H.; Hubbard, J.; Miller, M.; Rialon, K.; Kittrell, C.; Ramesh, S.; et al. Reversible, Band-Gap-Selective Protonation of Single-Walled Carbon Nanotubes in Solution. *J. Phys. Chem. B* **2003**, *107*, 6979−6985.
(39) Dukovic, G.; White, B. E.; Zhou, Z.; Wang, F.; Jockusch, S.; Steigerwald, M. L.; Heinz, T. F.; Friesner, R. A.; Turro, N. J.; Brus, L. E. Reversible Surface Oxidation and Efficient Luminescence Quenching in Semiconductor Single-Wall Carbon Nanotubes. *J. Am. Chem. Soc.* **2004**, *126*, 15269−15276.
(40) Zhou, W.; Vavro, J.; Nemes, N. M.; Fischer, J. E.; Borondics, F.; Kamarás, K.; Tanner, D. B. Charge Transfer and Fermi Level Shift in P-Doped Single-Walled Carbon Nanotubes. *Phys. Rev. B* **2005**, *71*, 205423.
(41) Engtrakul, C.; Davis, M. F.; Gennett, T.; Dillon, A. C.; Jones, K. M.; Heben, M. J. Protonation of Carbon Single-Walled Nanotubes Studied Using 13c and H 13c Cross Polarization Nuclear Magnetic Resonance and Raman Spectroscopies. *J. Am. Chem. Soc.* **2005**, *127*, 17548−17555.
(42) McDonald, T. J.; Engtrakul, C.; Jones, M.; Rumbles, G.; Heben, M. J. Kinetics of Pl Quenching During Single-Walled Carbon Nanotube Rebundling and Diameter-Dependent Surfactant Interactions†. *J. Phys. Chem. B* **2006**, *110*, 25339−25346.
(43) Korovyanko, O. J.; Sheng, C. X.; Vardeny, Z. V.; Dalton, A. B.; Baughman, R. H. Ultrafast Spectroscopy of Excitons in Single-Walled Carbon Nanotubes. *Phys. Rev. Lett.* **2004**, *92*, 017403.
(44) Lauret, J. S.; Voisin, C.; Cassabois, G.; Delalande, C.; Roussignol, P.; Jost, O.; Capes, L. Ultrafast Carrier Dynamics in Single-Wall Carbon Nanotubes. *Phys. Rev. Lett.* **2003**, *90*, 057404.
(45) Ellingson, R. J.; Engtrakul, C.; Jones, M.; Samec, M.; Rumbles, G.; Nozik, A. J.; Heben, M. J. Ultrafast Photoresponse of Metallic and Semiconducting Single-Wall Carbon Nanotubes. *Phys. Rev. B* **2005**, *71*, 115444.
(46) Yuma, B.; Berciaud, S.; Besbas, J.; Shaver, J.; Santos, S.; Ghosh, S.; Weisman, R. B.; Cognet, L.; Gallart, M.; Ziegler, M.; et al. Biexciton, Single Carrier, and Trion Generation Dynamics in Single-Walled Carbon Nanotubes. *Phys. Rev. B* **2013**, *87*, 205412.
(47) Spataru, C. D.; Ismail-Beigi, S.; Capaz, R. B.; Louie, S. G. Theory and Ab initio Calculation of Radiative Lifetime of Excitons in Semiconducting Carbon Nanotubes. *Phys. Rev. Lett.* **2005**, *95*, 247402.
(48) Jones, M.; Metzger, W. K.; McDonald, T. J.; Engtrakul, C.; Ellingson, R. J.; Rumbles, G.; Heben, M. J. Extrinsic and Intrinsic Effects on the Excited-State Kinetics of Single-Walled Carbon Nanotubes. *Nano Lett.* **2007**, *7*, 300−306.
(49) Park, J.; Deria, P.; Therien, M. J. Dynamics and Transient Absorption Spectral Signatures of the Single-Wall Carbon Nanotube Electronically Excited Triplet State. *J. Am. Chem. Soc.* **2011**, *133*, 17156−17159.
(50) Crochet, J. J.; Sau, J. D.; Duque, J. G.; Doorn, S. K.; Cohen, M. L. Electrodynamic and Excitonic Intertube Interactions in Semiconducting Carbon Nanotube Aggregates. *ACS Nano* **2011**, *5*, 2611−2618.
(51) Ma, Y.-Z.; Spataru, C. D.; Valkunas, L.; Louie, S. G.; Fleming, G. R. Spectroscopy of Zigzag Single-Walled Carbon Nanotubes: Comparing Femtosecond Transient Absorption Spectra with Ab Initio Calculations. *Phys. Rev. B* **2006**, *74*, 085402.